An Explicit Integration Framework for Nonlinear Analysis of Suspension Bridges

David B. McCallen[1] and Abolhassan Astaneh-Asl[2]

1. Director, Center for Complex Distributed Systems, Lawrence Livermore National Laboratory, Livermore, California, 94550, USA
2. Professor, Department of Civil and Environmental Engineering, University of California, Berkeley, California, 94720, USA, email: astaneh@ce.berkeley.edu

ABSTRACT: *In recent years computational simulation has taken an increased engineering importance in the seismic evaluation of critical structures. However, accurate nonlinear analyses of large suspension bridges continues to present earthquake engineers with a technically and computationally challenging problem. Application of general purpose nonlinear finite element software often results in computational models which are intractably large and computationally prohibitive. There are also specialized aspects to suspension bridges modeling, such as appropriate gravity initialization, that are not easily solved with general purpose computer programs. To address the simulation model challenges, a reduced order computational model has recently been developed for efficient nonlinear time history analysis. The model employs special element technologies tailored to suspension bridge applications and provides a hybrid implicit-explicit solution algorithm which can perform appropriate gravity initialization and adeptly handle extreme nonlinearties such as dynamic impact associated with pounding between bridge segments, foundation rocking or member buckling, and provide a framework which is readily migrated to a massively parallel compute environment. The computational model is described and a sample application is presented for the near-field seismic response of the San Francisco-Oakland Bay Bridge Western Crossing (USA).*

Keywords: Suspension bridge; Nonlinear analysis; E critical Structure; Hybrid implicit-explicit; algorithm; Seismic response; Oakland Bridge

1. Introduction

The design and analysis of major structures has become increasingly reliant on large-scale computational simulation. Linear simulations have been the mainstay of design computations, however, as performance based design procedures become more prevalent, there will be increased demand for accurate numerical models capable of simulating nonlinear response and ultimate structural instability.

The computational requirements for nonlinear seismic bridge analyses, which include changes in the global model geometry, impact between adjacent bridge segments, and material inelasticity, can be prohibitive if general purpose finite element programs are employed. This fact begs for efficient nonlinear computational models which will permit parametric studies essential to a clear understanding of bridge response and design optimizations.

In addition to computational difficulties, there continue to be phenomenological issues in the analyses of these important structures. The effects of spatially varying earthquake ground motions; near-field earthquake ground motions containing long-period ground displacement pulses and permanent ground displacements; and fluid-structure interaction between a bridges and the turbulent atmosphere, are topics for which scientific and engineering understanding are incomplete. Efficient and accurate simulation models will be essential to studying these complex phenomena.

There have been extensive analytical and numerical studies of the vibrational characteristics of cable supported bridges undergoing small amplitude, linear vibrations. The early work of Abdel-Ghaffar [1, 2, 3] provided basic understanding of the linear vibratory dynamics of suspension bridges. Abdel-Ghaffar's work constructed analytical models for the natural vibrations of suspension bridges and gave insight on the interactions between towers, cables, and deck systems. In a combined simulation and field observation study, Dumanoglu, Brownjohn,

and Severn [4] utilized two-dimensional and three-dimensional linear finite element models to investigate the natural vibrations of the Fatih Sultan Mehmet suspension bridge (Turkey) and extracted a large number of modes for the structure. Dumanoglu et al also performed transient analyses for multiple support earthquake excitations, concluding that variable support motion can lead to significantly larger forces than coherent support motions.

The first detailed experimental work on low amplitude, linear suspension bridge vibrations is contained in the study of Carder [5] in tests performed on the Golden Gate and San Francisco Oakland Bay Bridges (USA) in 1936. Carder employed a simple "Vibration-meter" consisting of a vibrating mechanical device recording on a strip of moving photographic paper. Carder periodically measured natural vibrations of bridge components during the construction of the bridges. The natural frequencies of the bridge components were inferred by examination of motion traces on the photographic plates. Carder's experimental tools were rudimentary in 1936, however, as discussed in subsequent sections, his experimental results appear to have yielded accurate modal data. Abdel-Ghaffar and Scanlon [6, 7] performed experimental investigations on the Golden Gate Bridge, in which 91 modes were identified in the range of 0-1.5*Hz* for the suspended structure, and 46 modes were identified in the range of 0-5*Hz* for the towers. The measured lower modes compared favorably with eigenvalues and eigenvectors obtained from a finite element model. Brownjohn, Damanoglu, and Severn [8] completed ambient vibration measurements on the Fatih Sultan Mehmet suspension bridge to identify mode shapes, frequencies, and modal damping. The observed modes correlated well with the lower modes computed from a finite element model, with increased divergence between observations and the model results at higher frequencies. Additional observational data is provided in the work of McLamore, Hart, and Stubbs [9] where experimental observations of the ambient vibrations of the Newport (USA) and William Preston Lane (USA) suspension bridges identified natural modes of vibration and corresponding modal damping values.

The existing experimental and modeling studies have generally demonstrated the ability of computational models to adequately represent the lower natural modes associated with small amplitude, linear vibrations. Due to the complexities and computational difficulties of large-scale nonlinear analyses, and a complete absence of measured response data in the strong motion earthquake regime, the effect of nonlinearities on cable bridge response has been investigated to a lesser extent. Abdel-Ghaffar and Rubin [10, 11] demonstrated the nonlinearity associated with modal coupling in amplitude dependent free vibrations of suspension bridges with application examples for the Golden Gate and Vincent Thomas bridges, and Nazmy and Abdel-Ghaffar [12, 13] have shown the important effect of geometric nonlinearities in cable stayed bridges. Consideration of nonlinearities in cable supported bridges is also beginning to infiltrate engineering practice, for example Ingham, Rodriguez and Nadar [14] describe design applications of nonlinear analysis in seismic retrofit studies of the Vincent Thomas Bridge (USA).

The objective of the work described in this paper was the development of a simple and robust computational model for three-dimensional, nonlinear analysis of suspension bridges. The resulting finite element model accounts for nonlinearities due to finite displacements, select material nonlinearities in the bridge members, impact between adjacent bridge segments, and potential rocking and uplift of large caisson foundations. The model provides a framework in which the most complex nonlinear behaviors, such as buckling of vintage built-up laced truss members, can be readily incorporated. Unique features of the model include the element technologies, which are tailored to the construction of a reduced-order model with a minimal number of global degrees of freedom; and the utilization of an explicit time-integration scheme for dynamic analyses. The explicit scheme provides a simple and highly reliable nonlinear time stepping framework for transient nonlinear analyses, which is especially effective for numerically capturing strong nonlinearities. The model incorporates an implicit based, automated procedure for nonlinear gravity initialization of the bridge model, which computes the correct bridge geometry and initial stress field in the cable and deck trusses for gravity loading.

2. Computational Bridge System Model

The research study motivating the development of the computational model consists of a multidisciplinary seismological and engineering case study of the San Franciso-Oakland Bay Bridge, see Figure (1). This 3400*m* long twin steel suspension bridge was built in the early 1930's and consists of a double deck system supported by steel trusses with laced members. With approximately 280,000 vehicles per day, this structure carries the highest traffic volume of any bridge in the world, it is a critical regional transportation link and a seismically interesting structure by virtue of its location in the near-field of two very active earthquake faults. A principal objective of the ongoing investigation is to assess the effects of long period, near-field earthquake motions on this spatially distributed flexible structure, an issue which has taken on pressing importance in light of recent observations of the long period content of near-field records in major earthquakes [15,16].

This paper describes and demonstraes application of the computational bridge model which has been developed. The description of the computaitonal model details

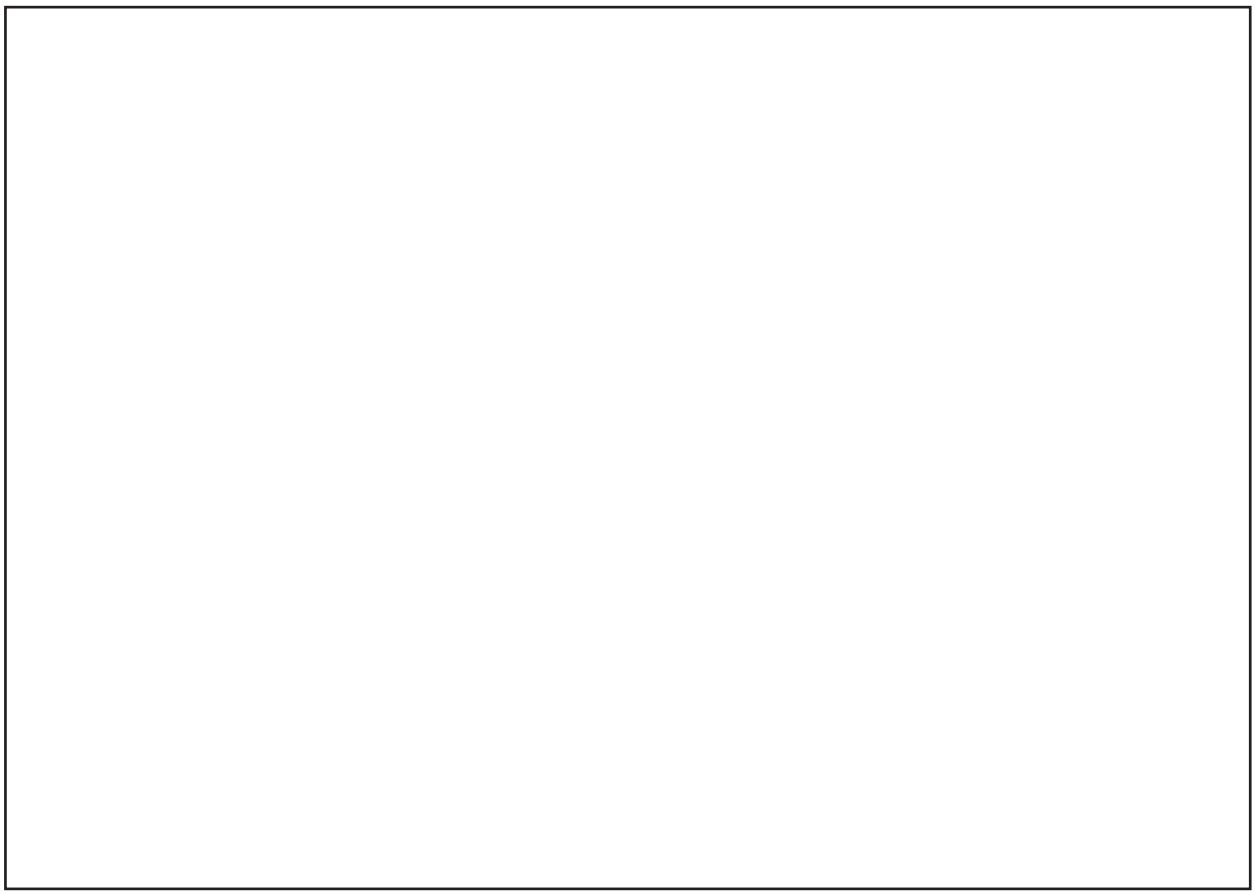

Figure 1. Seismological setting and the San Franciso-Oakland Bay Bridge Western Crossing. (a) Bridge location and nearby faults; (b) Twin suspension structures of the Bay Bridge Western crossing.

reference the application to the Bay Bridge system, however, the soulution algorithms and element technologies described have broader applicability to other cable supported bridges with appropriate changes in element properties.

The bridge model consists of the five basic elements, as shown in Figure (2). A reduced-order deck model, consisting of a composite combination of truss, membrane, and special sway stiffness elements represents the deck and stiffening truss system. A finite-rotation fiber bending element is used to represent the bridge towers. A penalty based node-to-node contact element captures potential contact and impact between the deck system and towers, and a rocking with contact foundation model represents the large caisson foundations including the potential for uplift. A tension-only cable element with user-defined initial stress represents the bridge cable system.

The philosophy in the development of the model was to maintain the greatest possible simplicity in the element formulations and solution algorithms, and to provide a robust algorithm which could handle a multiplicity of strong nonlinearities. An explicit time integration algorithm provides the required robustness for highly nonlinear dynamic problems. Explicit integration schemes are conditionally stable with the time step size governed by the highest frequency of the simulation model and with general purpose software this has historically resulted in too small a time step and too costly a solation procedure for long duration dynamic loads (e.g. earthquakes). On the other hand, the potential advantages of explicit integration are well known for highly nonlinear problems. These advantages include the basic simplicity and reliability of the algorithm when compared with the most efficient quasi-Newton implicit schemes. Explicit integration provides accuracy and high reliability for large nonlinear structures when extreme nonlinearities occur and can readily handle buckling or contact intensive problems which can significantly hamper convergence or degrade the economy of implicit integration schemes. Another major advantage of explicit methods, which is becoming more important with the emergence of massively parallel computers, is the ease with which explicit based programs can be migrated to a parallel compute environment. Explicit integration is computationally feasible for long duration problems if the element technologies and physical element sizes in the discretized model do not result in prohibitively small time steps. The special elements developed in this study result in manageable time steps and thus enable the use of explicit integration.

The nonlinear computational elements and algorithms developed have been incorporated into the special purpose finite element program *SUSPENDERS* at the Lawrence Livermore National Laboratory. A complete description, including detailed evaluations of element and software performance, is given in McCallen and

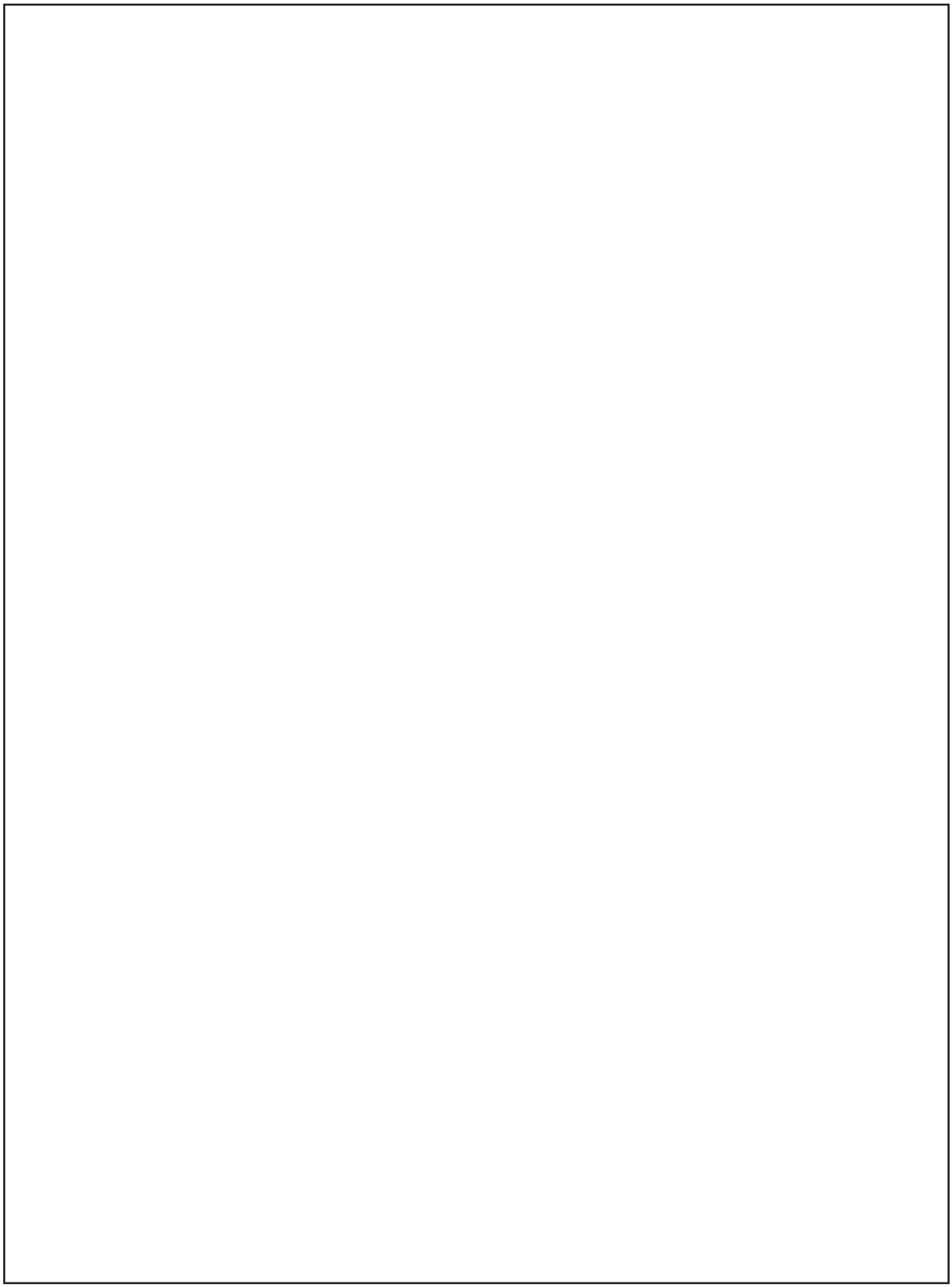

Figure 2. The five elements of the bridge system model. (a) Composite membrane, truss and sway stiffness deck model; (b) Finite rotation fiber flexure element for the bridge towers; (c) Caisson block with uplift; (d) penalty node-to-node contact for deck impact; (e)Tension-only two force member with initial stress for cables.

Astaneh-Asl [17].

3. Implicit/Explicit Global Solution Algorithms

In the numerical simulation of cable supported bridge systems subjected to dynamic loads, two distinct steps must be undertaken to obtain the transient solution. The first step is performance of a static, nonlinear gravity initialization such that the model obtains the correct geometric shape of the bridge with appropriate forces in the individual bridge deck members, towers, and cable system. This initialization must take into account the design objectives and construction sequence of the bridge as the construction procedure can significantly influence the gravity induced forces and the overall geometric shape of the bridge. Once the appropriate gravity configuration is achieved, the solution can proceed to the dynamic analysis with the static configuration (member forces and model geometry) serving as the initial condition state for the dynamic analysis.

3.1. Implicit Static Solution

In the computational model, the deformation of the bridge is defined by a vector of global displacement components $\{D\}$. For a given set of statically applied external loads on the structure $\{P\}$, the structure is in a state of equilibrium if the external loads equilibrate the internal resisting forces of the structure, denoted $\{Q(\{D\})\}$, and the forces generated by any contact across disjoint parts of the structure (e.g. expansion joints) and contact forces at the caisson/rock interface, denoted $\{\Gamma(\{D\})\}$. In a nonlinear system, the internal and contact forces are nonlinear functions of the system displacements. Defining a residual vector $\{R(\{D\})\}$ as the difference between the various force components in the direction of each degree of freedom of the model,

$$\{R(\{D\})\} = \{\{Q(\{D\})\} - \{P\} - \{\Gamma(\{D\})\}\} \quad (1)$$

an equilibrium configuration of the structure, denoted $\{D^*\}$, results in a null residual vector, i.e. $R\{D^*\} = 0$. If $\{D^k\}$ is the kth approximation to $\{D^*\}$, then a Taylor series expansion of the residual vector about $\{D^k\}$ yields,

$$\{R(\{D^*\})\} = \{R\{\{D^k\}\}\} + \left[\frac{\partial\{R(\{D^k\})\}}{\partial D}\right]\{\Delta D\} + o(\{\Delta D\}^2\rangle \quad (2)$$

where,

$$\left[\frac{\partial R}{\partial D}\right] = \begin{bmatrix} \left[\frac{\partial Q_1}{\partial D_1}\right] & \cdots & \left[\frac{\partial Q_1}{\partial D_n}\right] \\ \cdots & \cdots & \cdots \\ \left[\frac{\partial Q_n}{\partial D_1}\right] & \cdots & \left[\frac{\partial Q_n}{\partial D_n}\right] \end{bmatrix} - \begin{bmatrix} \left[\frac{\partial \Gamma_1}{\partial D_1}\right] & \cdots & \left[\frac{\partial \Gamma_1}{\partial D_n}\right] \\ \cdots & \cdots & \cdots \\ \left[\frac{\partial \Gamma_n}{\partial D_1}\right] & \cdots & \left[\frac{\partial \Gamma_n}{\partial D_n}\right] \end{bmatrix} \quad (3)$$

Neglecting higher order terms in Eq. (2), and invoking the fact that $\{R(\{D^*\})\} = 0$, the incremental displacements are given by,

$$\left[\frac{\partial\{R\langle\{D^k\}\rangle\}}{\partial D}\right]\{\Delta D\} = -\{R\langle\{D^k\}\rangle\} \quad (4)$$

The instantaneous stiffness matrix is defined as the immediate rate of change of the internal resisting and contact forces with respect to system displacements, thus,

$$[K_1(\{D^k\})] = \left[\frac{\partial\{R(\{D^k\})\}}{\partial D}\right] \quad (5)$$

and the individual terms of this matrix are given by Eq. (3). The first matrix in Eq. (3) represents the stiffness contribution from the structural elements in the bridge model; the second matrix in Eq. (3) represents the effective stiffness contribution from the penalty based contact elements activated during contact between disjoint parts. In the absence of contact, the contact stiffness matrix vanishes. The incremental relationship given by Eq. (4) provides the basis for equilibrium iterations which yield incremental displacements for updating the displacement vector until the nodal force residuals and incremental displacements become small. In the static solution algorithm, the instantaneous stiffness is completely reformed for each equilibrium interaction, leading to a full Newton-Raphson procedure for equilibrium iterations. Equilibrium iterations proceed until the Euclidean norms of the residual and incremental displacement vectors reduce below a prescribed tolerance. In the *SUSPENDERS* program, the implicit solution is utilized for gravity initialization of the bridge system, for other nonlinear static analyses such as push-over tests for a bridge or bridge components, and as a diagnostic tool when implementing new nonlinear elements.

3.2. Explicit Dynamic Solution

The transient bridge solution is based on an explicit integration scheme which readily admits multiple support earthquake ground motions. The earthquake ground motions are defined by ground displacement time histories at the bridge base support locations referenced to an identical time frame to preserve phasing information across the bridge structure. The coupled equations of motion for the bridge system, constructed from the assembly of element matrices, are given by,

$$[M]\{\ddot{D}(t)\} + [[C_{fsi}]\{\dot{D}(t)\} + [C_{mech}]\{\dot{D}_r(t)\}] + \{Q(\{D(t)\})\} + \{\Gamma(\{D(t)\})\} = \{P_{Boundary}(\{D_{q_i}(t)\})\} \quad (6)$$

where conceptually $[C_{fsi}]$ defines the damping due to fluid-structure interaction and $[C_{mech}]$ defines the mechanical damping. The vector $\{Q(\{D\})\}$ represents the internal resisting forces of the model elements, vector $\{\Gamma(\{D\})\}$ represents the nodal forces due to contact of disjoint bridge segments and caisson/rock contact, and $\{P_{Boundary}(\{D_{g_i}(t)\})\}$ contains the support point forces generated by applied ground displacements. In Eq. (6), the fluid-structure interaction damping forces are assumed proportional to the absolute velocity $\{\dot{D}(t)\}$ of the structure and the mechanical damping forces are assumed proportional to the relative velocity $\{\dot{D}_r(t)\}$ of the structure.

The specific form assumed for the bridge energy dissipation, as characterized by the viscous terms in Eq. (6), has significant implications for efficient implementation of the explicit integration procedure for the equations of motion. First, an appropriate damping form must be inferred from experimentally identified structural damping values. The most extensive and broad-band observational data on suspension bridge damping values is provided in the Golden Gate Bridge data of Abdel-Ghaffar and Scanlan [6, 7]. McLamore et al [9] identified the modal damping of the Newport and William Preston Lane Bridges, and Brownjohn et al [8] identified the damping of the first few modes of the Fatih Sultan Mehmet Bridge. The results of the modal damping observations from these studies are constructed in graphical form in Figure (3). In each plot, the experimentally observed damping values are shown as a function of frequency. The experimental data consistently exhibits an inverse relationship between modal damping and modal frequency, the only major difference between the various bridges being the specific amplitude of the damping values. In addition to the experimental values, a solid line is included for each dataset indicating the frequency dependency of damping which would be obtained with an assumption of mass proportional spectral damping (i.e. $[C] = \beta[M]$). For three of the cases (Golden Gate, Newport, and William Preston), the mass proportional damping was anchored at the fundamental mode; for the Fatih Sultan Mehment there was a wider scatter in the data and an anchor damping value lower than the damping of the fundamental mode proved to yield a better fit. For all of the small amplitude vibration data,

Figure 3. Experimentally observed damping in suspension bridges. (a) Golden Gate Bridge (length = 2738m); (b) Newport Bridge (length = 907m); (c) William Preston Lane memorial Bridge (length = 890m); (d) Fatih Sultan Mehmet Bridge (length = 1510m); (e) Damping overlay for all four bridges.

mass proportional damping provides a good representation of the observed frequency dependency of damping.

For mathematical expediency, and lacking more specific information about the mechanical and aerodynamic partitioning of the damping in cable bridges, an assumption of viscous, absolute velocity dependent damping was assumed in the computational model. Thus, Eq. (6) simplifies to,

$$[M]\{\ddot{D}(t)\}+[C][\{\dot{D}(t)\}+[Q(\{D\})]+\{\Gamma(\{D\})\} = \{P_{Boundary}(\{D_{g_i}(t)\})\} \quad (7)$$

In the course of this study, it was found that the use of strictly mass proportional damping resulted in unphysical high frequency chatter in the explicit computational model. This was an artifact of the extremely low damping which results in short wavelength, high frequency deck modes if mass proportional damping is used exclusively. Thus in practice it is necessary to augment the mass proportional damping with a small degree of stiffness proportional damping to ensure high frequency modes are appropriately damped, this issue is essential for explicit time integration where the higher frequency modes are resolved in the model. However, with explicit integration, the Courant stability time step is also adversely impacted by the damping in the highest frequency mode of the model [18]. If the damping in the highest frequency mode becomes large, the time step required to maintain stability decreases, resulting in excessive computational effort. In order to achieve the combined objectives of obtaining a decreasing damping with frequency (as indicated in the existing observation database), a small amount of damping in higher frequency modes to limit high frequency model chatter, and a low amount of damping at the very highest frequency modes to prevent excessive time step reduction, a three-term spectral damping representation was employed,

$$[C]=\alpha[M]+\beta[K]+\gamma[K][M]^{-1}[K] \quad (8)$$

This form of Caughey damping [19] provides a cubic variation of modal damping with frequency and the three coefficients in Eq. (8) can be selected to obtain the desired spectral damping characteristics.

With stiffness proportional terms included in the damping matrix, the matrix is non-diagonal and traditional finit differenceexperssions for the velocities must be modified to avoid a matrix inversion (Cook et al [18]). To avoid matrix inversions, and thus preserve the economy of the explicit integration scheme, the finite difference expressions become,

$$\{\dot{D}\}_n=\frac{1}{\Delta t}[\{D\}_n-\{D\}_{n-1}] \quad (9)$$

$$\{\ddot{D}\}_n=\frac{1}{(\Delta t)^2}[\{D\}_{n+1}-2\{D\}_n+\{D\}_{n-1}] \quad (10)$$

The backward difference in Eq. (9) (as apposed to a central difference) will result in slight accuracy loss in the integration scheme, which is generally insignificant for these structures due to the short time step of the explicit integration scheme.

Combining Eq. (7) through Eq. (9), and introducing seismic excitation as specified ground displacement time histories yields the recursion relationship for displacement,

$$\frac{1}{\Delta t^2}\{M\}\{D\}_{n+1} = \left\{\Delta t^2[M]^{-1}\{D_g\}_{n+1}\right\}-\{Q(\{D\}_n)\}-\{\Gamma(\{D\}_n)\}+ \frac{1}{\Delta t}\left[\frac{2}{\Delta t}[M]-\alpha[M]-\beta[K]-\gamma[K][M]^{-1}[K]\right]\{D\}_n+ \frac{1}{\Delta t}\left[\alpha[M]+\beta[K]+\gamma[K][M]^{-1}[K]-\frac{1}{\Delta t}[M]\right]\{D\}_{n-1} \quad (11)$$

where vector $\{D_g\}$ contains the earthquake ground motion displacement time histories at the individual bridge supports, the terms of which are zero except at the bridge support locations. For the Bay Bridge evaluation, the structure is founded on bedrock and the support displacement time histories were obtained directly from synthetic bedrock motions.

Eq. (11) provides the explicit recursion relationship for update of the structural model displacements. With the velocity approximation which has been invoked, and the fact that the model mass matrix is diagonal due to lumped mass assumptions, no matrix inversions are required for the solution of $\{D\}_{n+1}$. This explicit integration is conditionally stable, with the maximum time step permitted being governed by the Courant limit for the discretization of the particular bridge model at hand. The approximation invoked in Eq. (9) does slightly effect the stability time step, which must be accounted for in the selection of the integration step size [18].

For earthquake ground motions, there are two fundamental differences between the explicit algorithm defined in Eq. (11) and traditional seismic analyses methods. In the explicit formulation, ground motion is defined in terms of ground displacement time histories rather than acceleration time histories, and the computed displacement quantities are absolute displacements rather than displacements relative to the ground inertial reference frame.

4. Element Technologies

With careful construction and appropriate validation, it is possible to develop an accurate reduced-order model of a bridge system which captures the salient features of the dynamics of the system, yet results in a significant

reduction of the global degrees of freedom relative to a brute-force discretization with a general-purpose finite element program. The element development was aimed at significantly reducing the number of equations in the global bridge model. The Courant time step limit for stability of the explicit integration scheme depends on the transit time of a stress wave through the smallest elements in the bridge model and is thus a function of the physical dimensions of the elements in the computational model. To maximize the integration time step, an additional objective was to construct element technologies which allowed physically large element dimensions.

4.1. Tower Flexural Fiber Model

A fiber flexural element was developed for characterization of the bridge towers. The element incorporates both geometric and material nonlinearities. The framework for tracking geometry changes and initial stress inclusion are common to the bridge deck truss and cable elements described in subsequent sections, thus these features are discussed in some detail for the tower element to establish the element framework.

For three-dimensional bending with finite (large) rotations, the nonvectorial rotations must be incrementally updated. The flexure element utilizes three local element coordinate systems to track finite displacements and the finite rotations of the beam segments. Two local coordinate systems rotate and translate with the principal axes of the beam element at each end (the x", y", z", and x"', y"' and z"' axes in Figure (4)), a third updated Langrangian system (x', y', z') extends between the element end nodes and tracks the overall displacement and rotation of the element. A fundamental assumption of the element is that incremental rotations occurring between equilibrium iterations in the implicit solution procedure, or between time steps in the explicit dynamic solution, are small and can be transformed vectorially between the local coordinate systems. This assumption is easily met for practical problems, particularly with explicit integration where the time steps are small. The element also assumes the deformational rotations, for example the rotations between the x', y', and z' axes and the x", y", and z" axes, are small. Gross rigid-body rotations and translations are removed via the updated coordinate systems. To include the initial stress (geometric stiffness) contributions for the flexural element, which is required for gravity initiation of the bridge model, it is necessary to include all nonlinear terms in the strain-displacement relationships. To ensure efficiency of the element for linear as well as nonlinear problems, a cubic displacement field approximation was employed for the transverse displacements of the flexural element.

Inelasticity in the flexure element is accounted for by division of the cross section into a number of fiber zones with uniaxial plasticity defining the normal stress-strain relationship for each zone, as indicated in Figure (4). The element stress resultants are determined by integration of

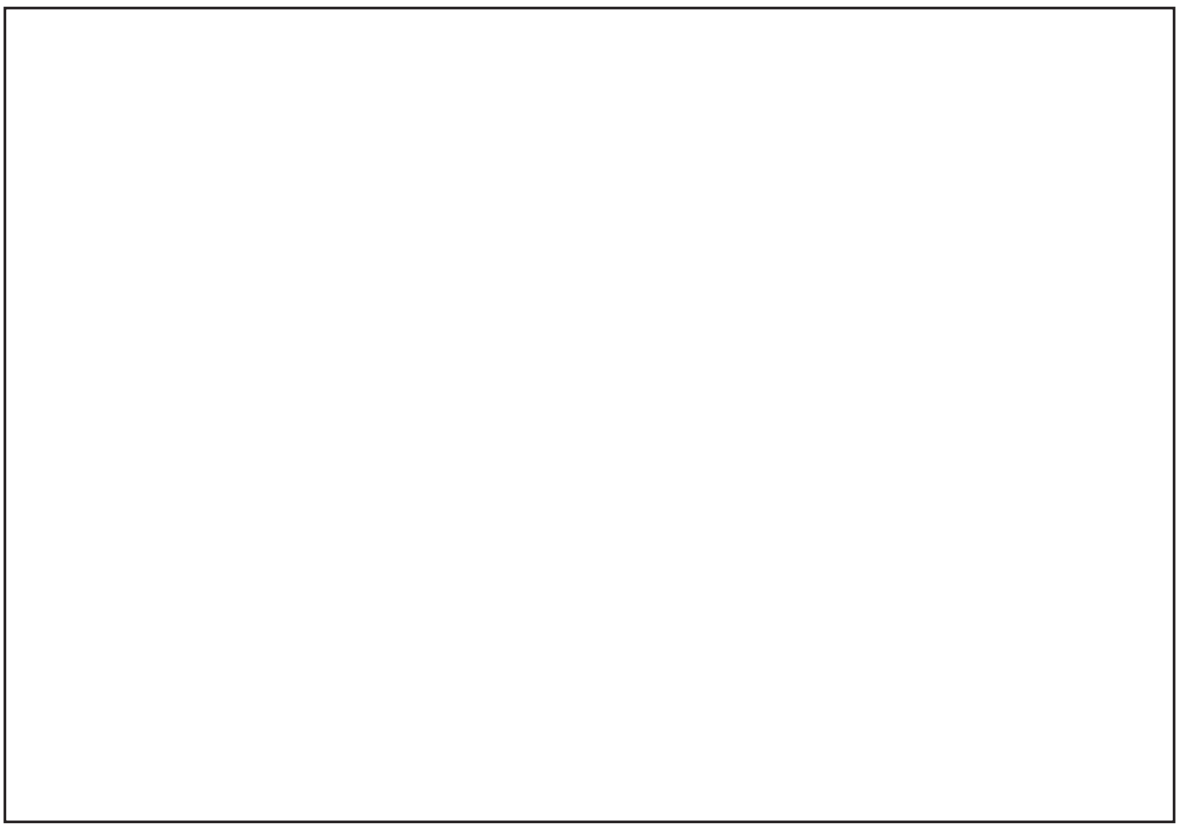

Figure 4. Finite rotation tower fiber flexure element.

the fiber zone stresses over the cross section of the flexural element. The evolution of the yield surface is monitored by tracking the center of the yield region, and a stress update algorithm was implemented to allow accurate integration of the stress-strain constitutive law for large strain increments, including full load reversals. To ensure path independence of the solution, the implementation of the plasticity model for the implicit Newton-Raphson equilibrium iterations employs a stress integration whereby the element stresses are updated from the last fully converged equilibrium state. The transformation between element local and global coordinates is accomplished through a vector translation of element forces and displacements based on the direction cosines of the current updated element coordinate system. Proceeding from a statement of virtual displacements [17], the flexural element matrices in natural coordinates are given by

$$\{Q_{Flexure}\} = [T]^T \int_{-1}^{1} [B]^T \{F\} J d\xi \tag{12}$$

$$\{K_{Flexure}\} = [T]^T \left(\int_{-1}^{1} [B]^T \left(\frac{\partial F}{\partial \varepsilon}\right) [B] J d\xi + \int_{-1}^{1} \left[\left[\frac{\partial}{\partial d_k} B_G(\{d\}) \right]^T \{F\} \right]_{k=1,12} J d\xi \right) [T] \tag{13}$$

where $[T]$ is the transformation matrix of direction cosines for the x', y', and z' coordinate system , $[B]$ is the linear strain-displacement matrix, $[B_G(\{d\})]$ is the displacement dependent strain displacement matrix resulting from the nonlinear strain terms, $[F]$ is the element stress resultants, and $\left[\frac{\partial F}{\partial \varepsilon}\right]$ is the element constitutive matrix. The second term of Eq. [13] represents the initial stress contribution to the element stiffness, and with appropriate mathematical manipulation [17], this matrix can be written as a function of the current axial force in the member. The element matrices are evaluated with a three point Lobatto quadrature integration which employs quadrature points at the extreme ends of the element. Lobatto integration captures inelasticity occurring at the ends of the element, where plasticity typically first initiates.

For earthquake simulations, the element stiffness is only required for the implicit iterations required for the model gravity initiation. After gravity initiation, the element internal resisting forces are computed from Eq. (14) for the explicit integration of the equations of motion.

The fiber element representation of the cellular Bay Bridge tower structure was assessed by comparison with detailed shell element based models and measured vibrational data. For this comparison, a detailed shell and beam element model was constructed for the general purpose finite element program *NIKE3D* [20], and a reduced-order fiber model was constructed for the *SUSPENDERS* program as shown in Figure (5). The detailed model used shell and beam elements to represent the laced members in the tower diagonals and struts, and discretized the internal cellular structure of the tower including the transverse stiffening diaphragms. The fiber model employs one fiber zone for each cell segment in the tower, for example, the element uses 62 zones at the base of the tower.

The first six natural modeshapes of the tower, as computed by detailed and reduced-order models, are shown in Figure (5) along with selected tower frequencies experimentally measured by Carder in 1936. Carder performed vibrational measurements of the Bay Bridge towers when the tower construction was completed and the towers were free standing prior to spinning of the main cables.

The reduced-order-model provides good estimates of the tower dynamics, and in light of the potential errors in the measured data, there is good agreement between the numerical models and the experimental data of Carder.

4.2. Reduced-Order Deck Model

A truss bridge deck system can demand a prohibitive number of elements with brute force modeling based on shell and beam elements. An effective reduced-order model, which exploits the specific configuration of suspension bridges, can dramatically reduce computational effort. The representation of a three-dimensional discrete lattice truss structure by an equivalent beam-like continuum has seen wide use in the development of reduced order models. Abdel Ghaffar [3] utilized this approach in the development of linear models for suspension bridge dynamics, and McCallen and Romstad [21] developed continuum models for lattice structures, including both geometric and material nonlinearities. For certain bridge deck configurations, beam-like continua models can adequately characterize the stiffening truss system in the mid-deck region of the structure. However, the ability of continuum based models to capture the localized effects of complex articulations at the ends of the stiffening trusses is highly suspect (Avent and Issa [22]). Accurate continuum representations also become problematic when the bridge deck system lacks transverse sway bracing, and the deck is subjected to significant complex warping deformation. Warping deformations defy attempts to represent the deformations with simple beam-like kinematics. The deck model which has been developed represents a compromise between a highly efficient, but questionably accurate, continuum model of the deck system and a prohibitively expensive brute force discrete shell and beam element model of the deck.

An accurate reduced-order model of the deck for a particular bridge must take into consideration the specific construction details and load paths in the deck system. The configuration and connection details in the two-level deck system of the Bay Bridge made appropriate reduced-order model construction particularly challenging. Lacking transverse sway bracing between the upper and lower decks, see Figure (6), forces generated between

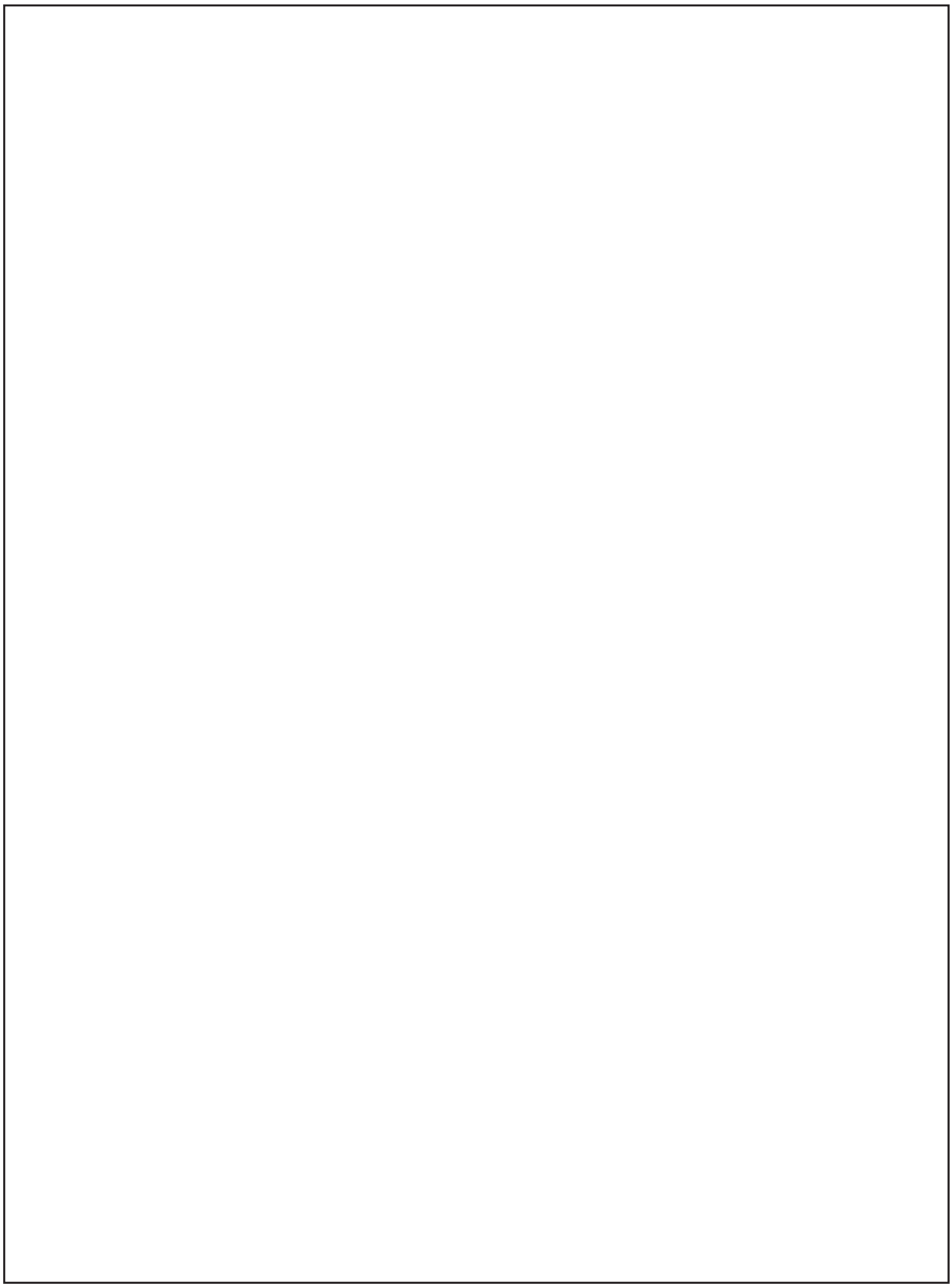

Figure 5. Detailed shell and beam element and reduced order fiber bending element tower models and computed modeshapes (experimental values shown parenthetically).

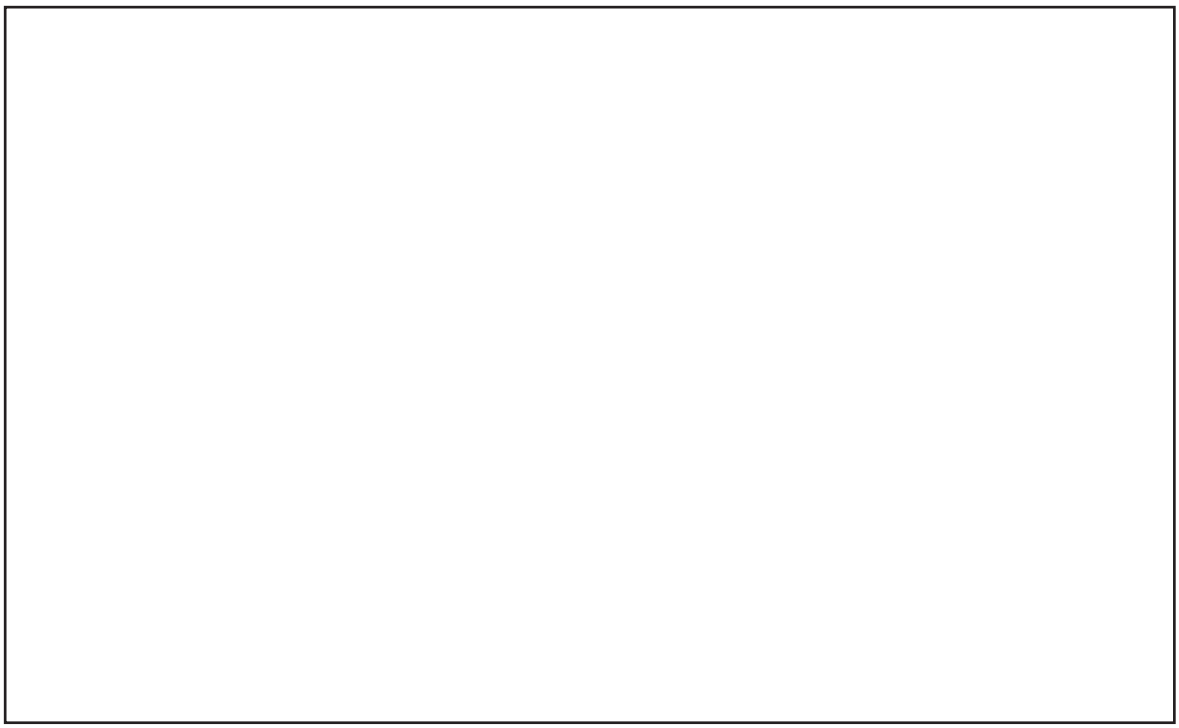

Figure 6. Reduced order model of the deck system. (a) Sway stiffness element; (b) Slab membrane; (c) Stiffening truss element (all elements shown in local element updated Lagrangian coordinate systems).

the upper and lower decks must be transferred through bending of the stiffening truss elements in an inter-deck sway deformation. In the longitudinal direction, the deck slab-to-stiffening truss connection occurs through weak axis bending of the deck beams shown in Figure (7), providing a very flexible connection between the deck slabs and the stiffening trusses. The deck roadway system, consisting of the concrete slab, deck beams, and stringers, are weakly coupled to the deck stiffening truss in the longitudinal direction of the bridge, and the full membrane stuffinesses of the deck slabs are not activated by transverse and vertical deformations of the stiffening trusses. The complex kinematic characteristics associated with deck cross-section warping of this particular deck do not readily lend this system to accurate characterization with beam-like continua.

The reduced-order deck model constituents consist of simple truss elements for the stiffening truss members, an orthotropic plane stress element for the deck slab and girder system, and a sway-stiffness element to account for the transverse bending of the lateral frames composed of the deck beams and stiffening truss vertical posts, as shown in Figure (6). The active global degrees of freedom consist of three translations at each joint of the deck system. The sway-stiffness element was implemented to eliminate the need for any rotational degrees of freedom in the deck model. The capability to accommodate geometric nonlinearities associated with arbitrarily large displacements was included to capture the effects of large displacements which can occur in a long bridge during earthquake motions. Depending on the bridge system, and the method by which the model is initialized to achieve the appropriate gravity configuration, gross model geometry changes and large model displacements must also be accommodated for gravity initialization of the bridge model.

The deck truss element shares common features with the flexural fiber tower model element in terms of the methodology for including geometric nonlinearities, displacement tracking, and elasto-plastic inelasticity. Similar to the tower flexure element, the member motions are tracked with a local element updated Lagrangian coordinate system which translates and rotates with the element through space. For the static initialization sequence, it is necessary to include the geometric component of element stiffness for select truss elements to create a nonsingular initial global stiffness matrix which allows equilibrium iterations to proceed. To include the initial geometric stiffness, the user must provide as input an initial axial tension in selected members of the deck stiffening truss system. For the Bay Bridge configuration, for example, an initial tension must be input for all of the vertical posts of the deck trusses.

A classical elasto-plastic representation provides an appropriate approximation for modern bridge members where members and connections are based on sound inelastic design methods. For some vintage steel laced members, recent experimental research [23] indicates the nonlinear behavior can be controlled by very complex inelastic buckling of the member or gusset plate connections. The incorporation of complex inelastic buckling of vintage laced members and connections will be addressed

in future *SUSPENDERS* developments and incorporated in the nonlinear material library as appropriate closed form representations of buckling laced members and pusset joints are developed.

The deck membrane element, which represents the deck slab, beams, stringers, and any existing in-plane sway bracing, consists of a four node, isoparametric, orthotropic plane stress element. Potential large rigid-body displacements of the element are accounted for with an updated coordinate system which tracks with the element through space, as indicated in Figure (7). The element matrices are based on a classical four node isoparametric formulation. Selection of appropriate membrane properties was a difficult problem in the development of the reduced-order model for the Bay Bridge deck system because of the weak coupling between the deck slabs and stiffening trusses, see Figure (7). The deck membranae element requires elastic constants which characterize the equivalent stress-strain behavior of the deck system, because of the complex deformations in the deck/truss interaction, effective membrane properties cannot be easily obtained with simple first principal analytical solutions. For the Bay Bridge model, the equivalent membrane elastic properties were computed numerically by selective loading of detailed models of deck segments, see Figure (7). The detailed deck models shown in Figure (7) were constructed to include the weak connection between the deck system and the stiffening truss chords. The effective membrane properties are obtained from the detailed model analysis, for example the longitudinal membrane effective elastic modulus is given by

$$E_{effective} = \frac{\frac{PL}{\Delta_1} - 2(EA_{chords})}{A_{membrane}} \tag{14}$$

where Δ_1 is the stretch of the deck system for an applied load of P. After determining the appropriate elastic constants, the membrane element contribution to the

Figure 7. Deck membrane element. (a) Element degrees of freedom and updated Lagrangian coordinate system; (b) Upper and lower deck in-plane models and equivalent membrane.

element internal resisting forces and instantaneous stiffness are given by McCallen and Astaneh-Asl [17]

$$\{Q_{Membrane}\}=\left[\int_{-1}^{1}\int_{-1}^{1}[B]^T[E][B]tDetJd\xi d\eta\right]\{d\} \quad (15)$$

$$\{K_{Membrane}\}=\int_{-1}^{1}\int_{-1}^{1}[B]^T[E][B]tDetJd\xi d\eta \quad (16)$$

where [*E*] contains the effective material constants obtained from the detailed deck segment models. Classical four point Gaussian quadrature integration is employed for the natural coordinate integration of the matrices.

The sway-stiffness element accounts for the lateral sway deformation between the upper and lower decks resulting from flexure of the frame consisting of the deck beams and stiffening truss vertical posts. In the deck model the sway stiffness element is an 8 by 8 stiffness matrix which relates nodal forces to the lateral sway deformation of the frame. The element contains four nodes with two in-plane displacements per node and is placed in the deck model in addition to the truss elements which represent the axial stiffnesses of the individual truss posts and deck beams. The sway and truss elements are shown in Figure (8). The sway deformation between the decks is approximated by the summation of angles γ_1 and γ_2

$$\gamma_{sway}=\gamma_1+\gamma_2 \quad (17)$$

where

$$\gamma_1=\left(\left(\frac{d_4+d_6}{2}\right)-\left(\frac{d_8+d_2}{2}\right)\right)/W \quad (18)$$

$$\gamma_2=\left(\left(\frac{d_5+d_7}{2}\right)-\left(\frac{d_3+d_1}{2}\right)\right)/H \quad (19)$$

The nodal forces associated with sway deformation can be obtained analytically or numerically by analysis of the cross section frame with the loading and boundary conditions shown in Figure (8). For elastic behavior of the frame, the nodal forces associated with sway are given by

$$\begin{bmatrix}F_H\\F_V\end{bmatrix}=\begin{bmatrix}k_h\\k_v\end{bmatrix}\gamma_{sway} \quad (20)$$

Combining Eq. (17) through Eq. (20), and utilizing overall equilibrium relationships between the nodal forces in Figure (8), the sway element stiffness matrix is given by

$$\begin{bmatrix}q_1\\q_2\\q_3\\q_4\\q_5\\q_6\\q_7\\q_8\end{bmatrix}=\frac{k_h}{2D}\begin{bmatrix}1&\eta&1&-\eta&-1&-\eta&-1&\eta\\ \eta&\eta^2&\eta&-\eta^2&-\eta&-\eta^2&-\eta&\eta^2\\ 1&\eta&1&-\eta&-1&-\eta&-1&\eta\\ -\eta&-\eta^2&-\eta&\eta^2&\eta&\eta^2&\eta&-\eta^2\\ -1&-\eta&-1&\eta&1&\eta&1&-\eta\\ -\eta&-\eta^2&-\eta&\eta^2&\eta&\eta^2&\eta&-\eta^2\\ -1&-\eta&-1&\eta&1&\eta&1&-\eta\\ \eta&\eta^2&\eta&-\eta^2&-\eta&-\eta^2&-\eta&\eta^2\end{bmatrix}\begin{bmatrix}d_1\\d_2\\d_3\\d_4\\d_5\\d_6\\d_7\\d_8\end{bmatrix} \quad (21)$$

or

$$\{q\}=[k_s]\{d\} \quad (22)$$

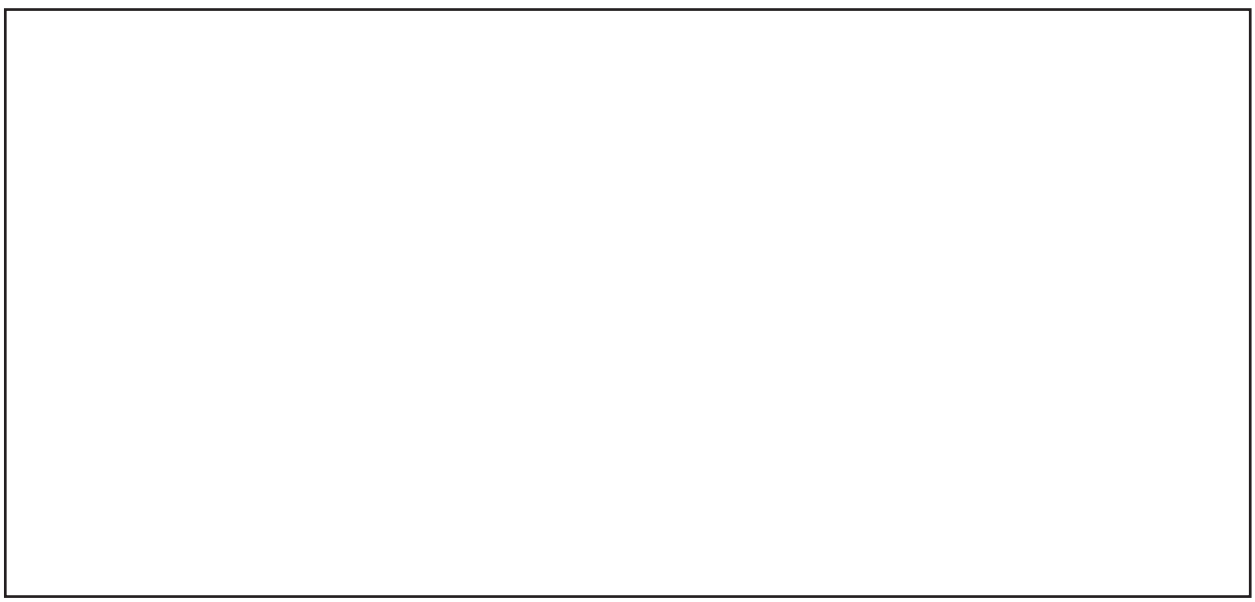

Figure 8. Sway stiffness element providing lateral sway resistance. (a) Sway and truss elements; (b) Determination of sway element nodal forces for a sway displacement.

where $\eta = \frac{H}{W}$. An updated Lagrangian coordinate system tracks with the element to remove large rigid-body displacements. Eq. (21) provides the sway element nodal forces in terms of the nodal displacement quantities. The element matrices in global coordinates are provided by the transformation between the element instantaneous updated Lagrangian system and the global system coordinates

$$[Q_{sway}] = [T(\{d\})]^T [k_s] \{d\} \tag{23}$$

$$[K_{sway}] = [T(\{d\})]^T [k_s] [T(\{d\})] \tag{24}$$

To evaluate the accuracy of the reduced order deck model, a number of comparisons were made between the reduced-order deck model and a detailed beam and shell element model of the Bay Bridge deck system. The first five modes of a simply supported twenty bay segment of the Bay Bridge deck, as computed from detailed and reduced-order models, are shown in Figure (9). The mode shapes computed with the two models exhibited excellent

Figure 9. Natural modeshapes of a twenty bay deck segment form detailed and reduced order models.

correlation, and the frequencies are within approximately 10 percent for all of the first five modes.

4.3. Bridge Cable Model

Bridge cables are represented with a simple tension-only two-force member in which the cable element coding does not permit compression to develop in any cable element. If the cable element attempts to compress, the element stiffness and residual contributions are neglected in the implicit solution and the element forces are neglected in the explicit solution. An initial stress contribution to the element instantaneous stiffness is included to render the initial global tangent stiffness matrix of the model non-singular during gravity initialization. The procedure developed to define the initial geometry of the cables is based on constraining the cables by the initial unstretched cable length and allowing the Newton-Raphson equilibrium iterations to determine the natural sag geometry and tension of the cables. With the initial unstretched length of each cable serving as the constraint for the cable system model, the definition of the starting cable geometry in the finite element model is arbitrary and only affects the number of equilibrium iterations required to achieve the natural sag.

A *SUSPENDERS* program simulation of a simple sagging cable experiment by Irvine and Sinclair [24] based on this approach is illustrated in Figure (10). The initial geometry in the finite element model is crudely represented with two prescribed linear segments of cable elements, the total length of which exactly equals the unstretched length of the actual cable. A uniform initial tension guess is applied as user input to each cable element for initialization of the initial stress contribution, and once gravity is applied, full Newton-Raphson equilibrium iterations achieve the appropriate cable geometry rapidly within five equilibrium iterations. The individual cable elements displace through large rigid-body displacements, and the overall geometry rapidly progresses to the appropriate hanging cable geometry. The numerical simulation results precisely matched experimental data for the hanging cable obtained by Irvine and Sinclair. Application of a point load was also considered after gravity initialization to emulate Irvine and Sinclair's experiment and the simulation model accurately computed the deformed shape under gravity plus point loading, as shown in Figure (10).

In the case of the Bay Bridge, the design and construction objectives included achieving a stress state in which the chords and diagonals of the stiffening truss were stress

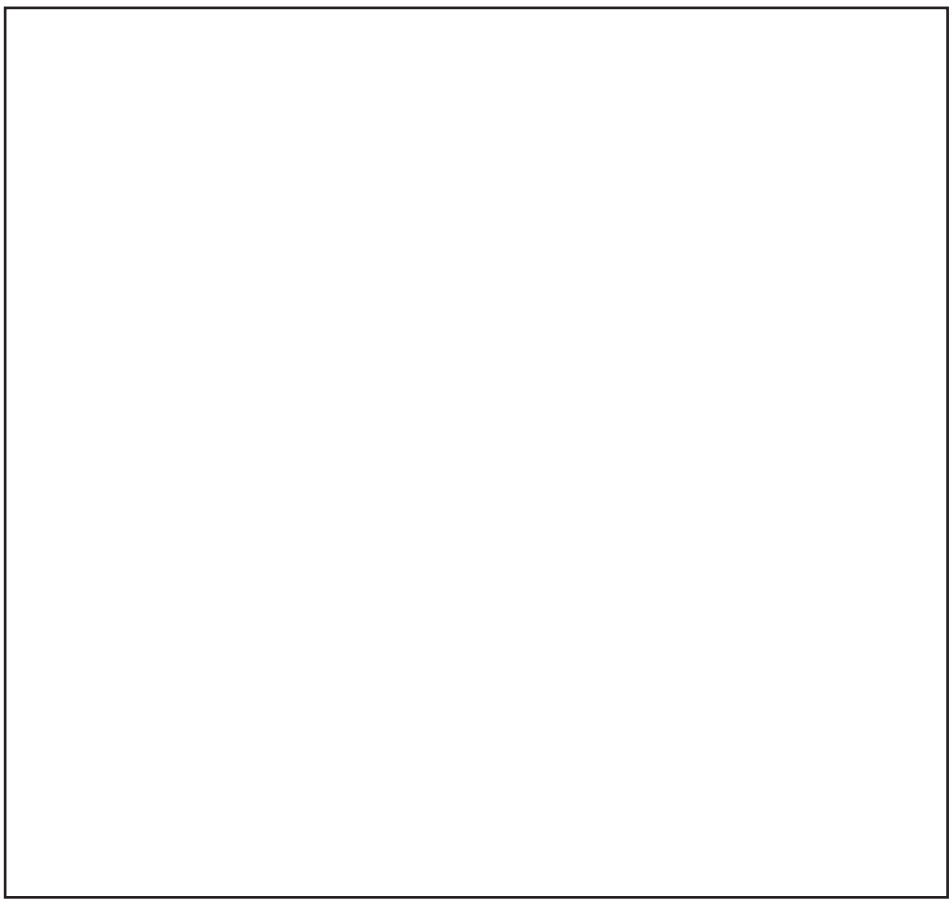

Figure 10. Analysis of a hanging cable. (a) Ten element cable model with initial tension and constrained length; (b) Deformed shape at each equilibrium iterations; (c) Computed and observed cable geometry under gravity and point load; (d) Computed and observed cable geometry under gravity and point load.

free under full gravity dead load. The vertical posts of the truss were the only gravity stressed members in the deck truss. This condition was obtained in field construction by allowing the truss joints to remain loosely tacked together with construction pins until the deck was entirely supported from the vertical suspenders, with final riveting of the joints after the entire deck was suspended. As a result of this construction sequence, the deck stiffening truss did not resist the bridge's gravity load as a composite structure. This design objective is common for many lattice deck suspension bridges. On the Bay Bridge, hydraulic jacking was also employed between the main cables and the cable saddles atop the towers prior to application of the deck system to ensure the towers would be straight, vertical, and free of shear forces and bending moments at the completion of the construction sequence.

The computational procedure for model initialization must emulate this construction sequence. To initialize the bridge model to the appropriate gravity configuration, an automated procedure was developed. The procedure first analyzes the main cables and towers under full bridge dead load to determine the final main cable elevations under full gravity load (Figure (11b-c)). For this analysis, the unstretched length of the main cables is required, and it can be estimated from the design documents or cable surveys obtained during bridge construction (Figure (11a)). Based on the nodal locations from the dead-load analysis and the final design elevations of the deck system, the unstretched length of the vertical suspenders is computed and the initial nodal locations of the deck nodes are determined, see Figure (11d). This provides the information necessary for constraining the definition of the initial undeformed bridge model geometry. The implicit nonlinear solution procedure is then used with Newton-Raphson equilibrium iterations until the gravity load geometry and stress field are achieved.

With the current availability of powerful finite element mesh generators, it is computationally expedient to generate a starting model with a parabolic approximation to the main cable geometry. For most suspension bridges, the parabolic approximation provides a geometry close to the correct gravity shape. In the Bay Bridge model generation, the parabolic shape is computed such that the main cables have the appropriate unstretched length, and the initial location of the deck nodes are determined by dropping to an elevation corresponding to the unstretched length of the vertical suspenders. The chord and diagonal elements of the truss are inactivated for the gravity initialization, so the deck truss will not contribute stiffness to the model during application of gravity loads. In addition, the main cables are allowed to slip horizontally relative to the tops of the towers, so the towers will be straight and subjected to pure axial load at the end of gravity initialization. Once the gravity load equilibrium iterations are complete, new truss diagonal and chord element lengths are computed and stored automatically by the *SUSPENDERS* program so that these members are unstressed under the gravity loads. The gravity deformed shape and tension stress fields obtained from the static analysis become the initial condition state for the transient earthquake computation. Once the appropriate gravity load configuration is achieved, the main cables, which were allowed to slip relative to the towers under gravity initialization to keep the towers vertical and absent of longitudinal shear loads (per the construction sequence), are slaved to the top of the towers to provide cable-to-tower connectivity for the transient response analysis. The model developed for half of the Bay Bridge geometry is shown in Figure (12). This model initialization procedure ensures that the bridge computational model will have the correct as-built bridge geometry, including the appropriate vertical curve in the main span and the appropriate grade in the side spans. The cables have the correct geometric shape and gravity load tensions, the towers will be vertical and subjected to only axial forces, and the stiffening truss diagonals and chords will also be stress free at the end of gravity initialization as required to emulate the as-built design objective.

4.4. Deck and Caisson Contact Models

Bridge deck systems typically contain a number of structural discontinuities at interior expansion joints and at abutments to accommodate thermal deformations. These discontinuities can have a pronounced influence on the dynamic response of the bridge system and can result in significant dynamic impact between disjoint bridge segments. Observational measurements of the earthquake response of bridges have indicated the occurrence of large accelerations and intersegment forces as a result of impact of adjacent bridge segments [25]. In addition to deck segment impact, unanchored bridge foundations can potentially be subjected to rocking and uplift, with multiple occurrences of impact. For the Bay Bridge, the towers are placed on large caissons which rest on bedrock, the caissons are unanchored to the bedrock, and the potential exists for rocking and uplift of the caissons under strong ground motion. Foundation rocking can significantly effect the superstructure response to earthquake ground motions [26] and should be accounted for in an accurate numerical simulation.

To simulate deck impact and foundation rocking, a simple node-to-node contact element was developed for the *SUSPENDERS* program which allows two nodes to close within a specified stand off distance before contact occurs. The element also admits tensile forces to develop between the nodes as the nodes separate to allow representation of displacement-limiting structural details which

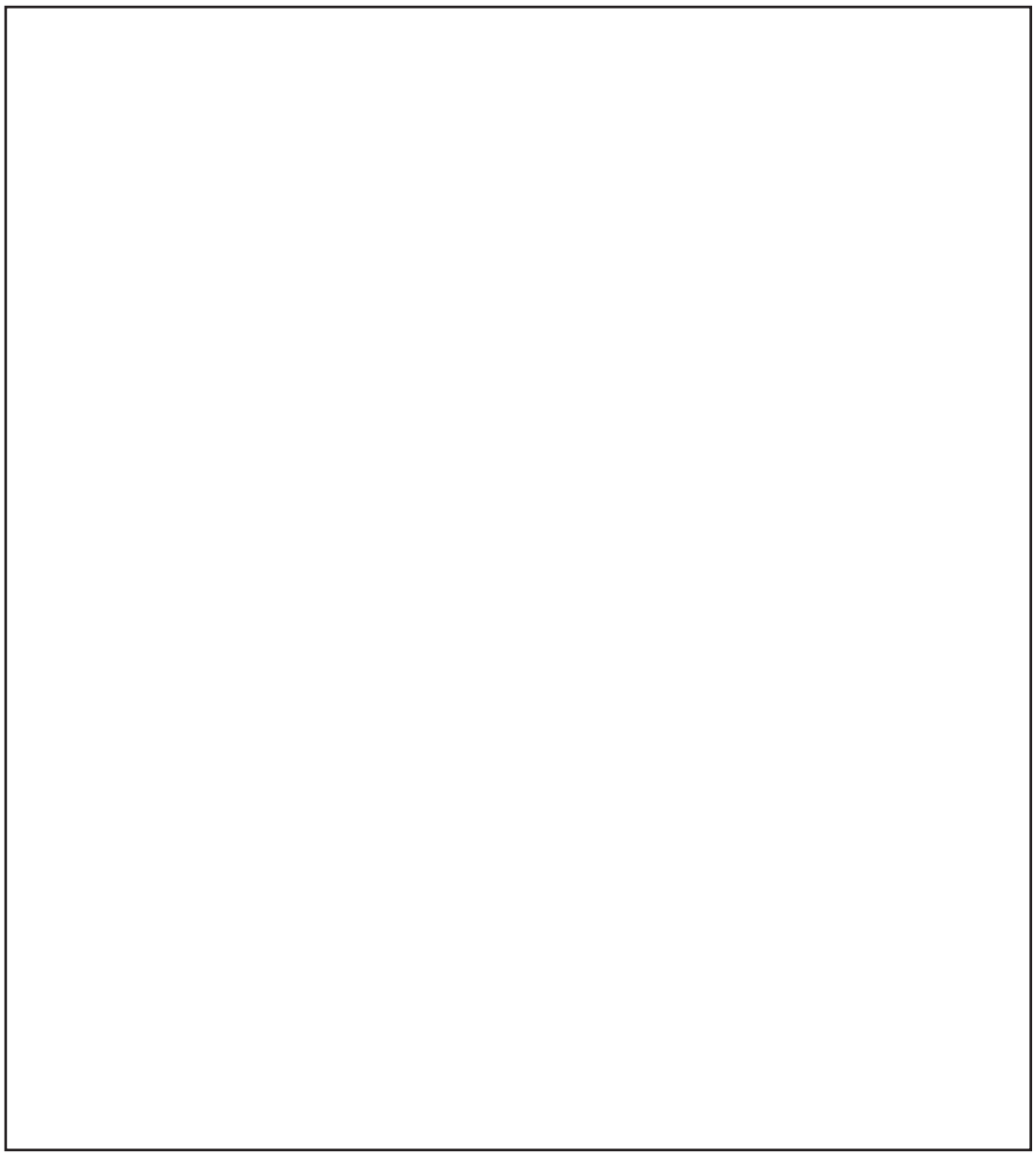

Figure 11. Development of a model with appropriate gravity shape and forces. (a) Estimate unstretched length of main cables based on bridge design and cable field survey data; (b) Generate simple model geometry with the appropriate unstretched engths; (c) Perform static load analysis of main cables with full dead load of deck system; (d) Based on computed main cable geometry and design deck elevations, determined stretched lengths of suspenders under gravity load, (e) Generate a model with arbitrary geometry constrained by unstretched cable lengths; (f) Perform implicit Newton-Raphson equilibrium iterations for gravity loads until convergence.

can prohibit large separation of two bridge segments. For the Bay Bridge, the main suspended spans are connected to the towers and central anchorage caisson with a slip joint that couples the deck to the tower or caisson in the transverse direction, but allows limited longitudinal motion once static friction of the joint is overcome, as shown in Figure (13). This construction detail can be compressive when the deck moves into the caisson or tensile when the deck pulls away from the caisson.

In the node-to-node contact element, the nodal force contributions are generated vectorially and translated into the global bridge geometry based on the current deformed shape of the bridge system. The contact forces are given by

$$\begin{bmatrix} \Gamma_1 \\ \Gamma_2 \end{bmatrix} = K_C \left[\begin{bmatrix} 1 & -1 \\ -1 & 1 \end{bmatrix} \begin{bmatrix} d_1 \\ \\ d_2 \end{bmatrix} + \begin{bmatrix} -1 \\ 1 \end{bmatrix} \delta_C \right] (\psi_C(d_2, d_1, \delta_C)) + K_T \left[\begin{bmatrix} 1 & -1 \\ -1 & 1 \end{bmatrix} \begin{bmatrix} d_1 \\ \\ d_2 \end{bmatrix} + \begin{bmatrix} 1 \\ -1 \end{bmatrix} \delta_T \right] (\psi_T(d_2, d_1, \delta_T)) \quad (25)$$

where

$\psi_C(d_2, d_1, \delta_C) \equiv 1.0$ when $((d_1 - d_2) - \delta_C) > 0$ and
$\psi_C(d_2, d_1, \delta_C) \equiv 0$ when $((d_1 - d_2) - \delta_C) \leq 0$,

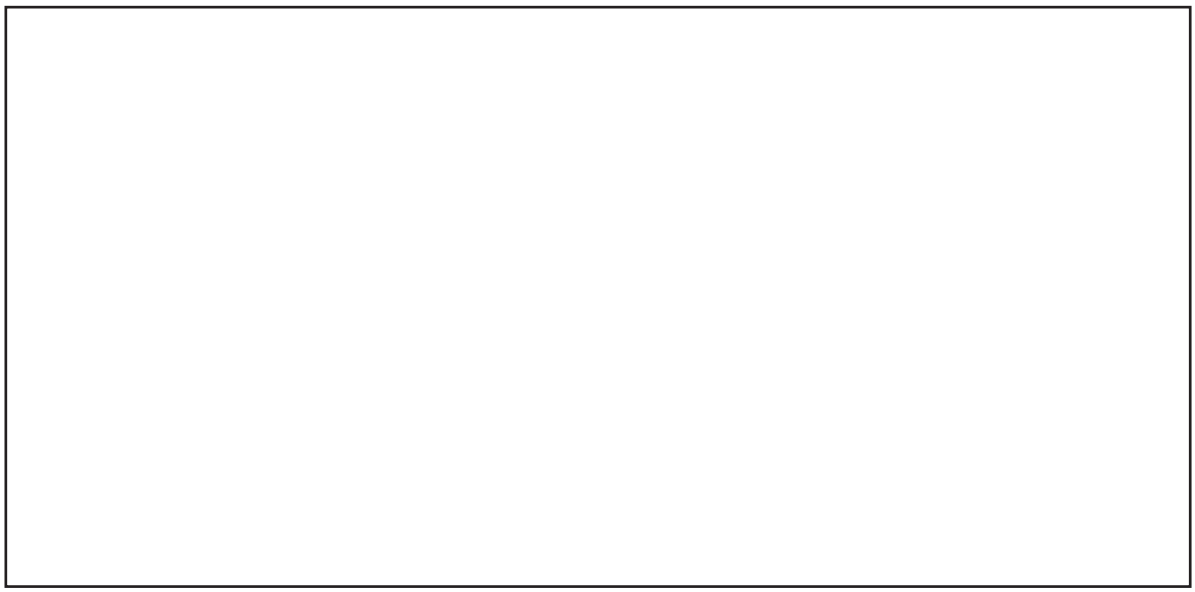

Figure 12. Gravity initialization of the model with different initial model geometries.

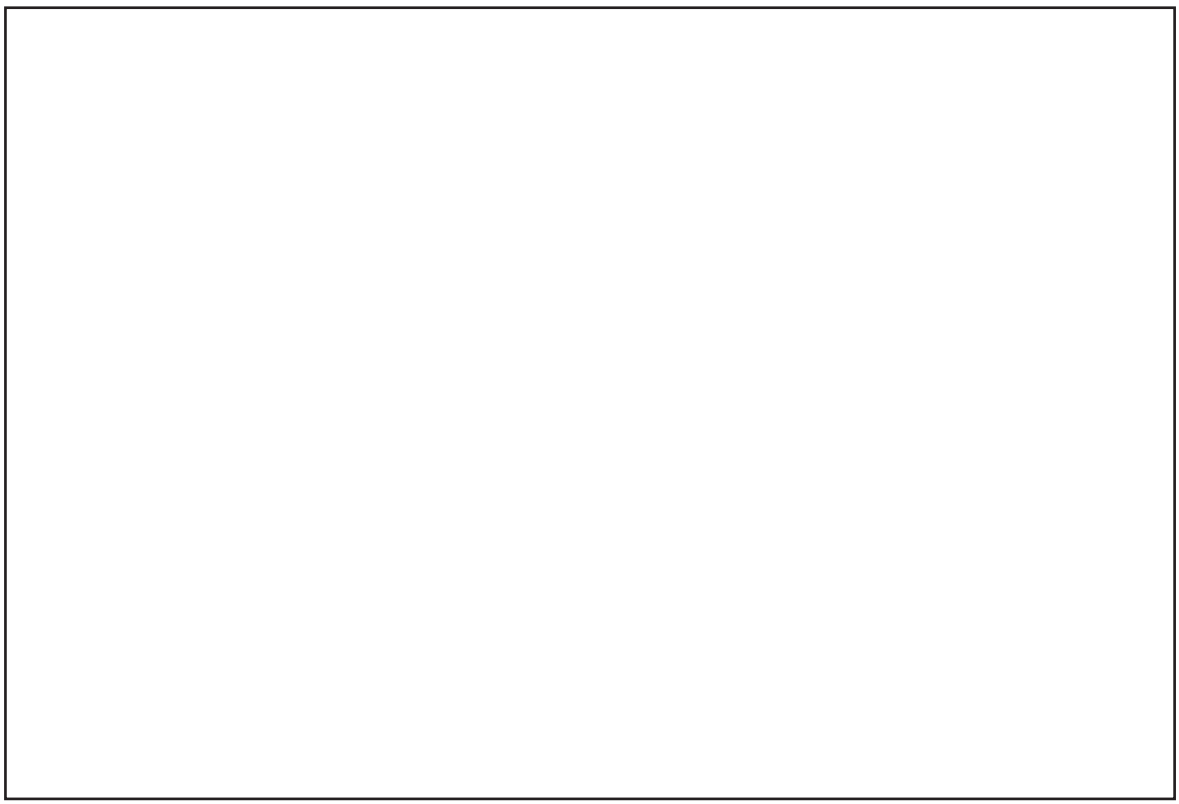

Figure 13. Nodal contact in the bridge model. (a) Contact at the deck-to-tower and deck-to-caisson connection; (b) Contact at the base of a caisson.

$\psi_T(d_2, d_1, \delta_T) \equiv 1.0$ when $((d_2 - d_1) - \delta_T) > 0$ and
$\psi_T(d_2, d_1, \delta_T) \equiv 0$ when $((d_2 - d_1) - \delta_T) \leq 0$

The nodal contact forces are directed colinear along the line defined by the two contact nodes (Node *I* and Node *J* in Figure (13)) and can be transformed to global coordinates based on the direction cosines of the line segment.

Pounding between bridge segments or foundation rocking with impact can result in abrupt nonlinearities in the bridge system model. There have been many simple approximations to contact with various quasi-linearized gap elements, which are highly suspect in their ability to accurately represent violent, sudden impacts. Based on the authors' practical experience with implicit time integration finite element programs, the seismic analysis of large bridges with multiple impacting segments can be quite challenging with many equilibrium iterations and potential converge failure for each severe impact event. At best, recurring pounding significantly detracts from the

efficiency of implicit time integration schemes. Explicit time integration, on the other hand, is particularly adept at accurately tracking impact events, with no detriment to the algorithm efficiency when severe pounding occurs.

5. Example Application: Bay Bridge Response to Near-Field Earthquake Ground Motions

Once a bridge model is appropriately initialized under gravity loading, eigenvalue analyses can be performed to determine the natural modeshapes and frequencies of the structure and the time history response to earthquake ground motion can be computed. Selected natural modes of the Bay Bridge obtained from the *SUSPENDERS* program are shown in Figure (14). The fundamental mode consists of transverse motion of a main span and this concurs with the fundamental mode observed by Carder in this 1936 field study. The computed modal period also agrees quite well with the period Carder measured in his instrumentation survey.

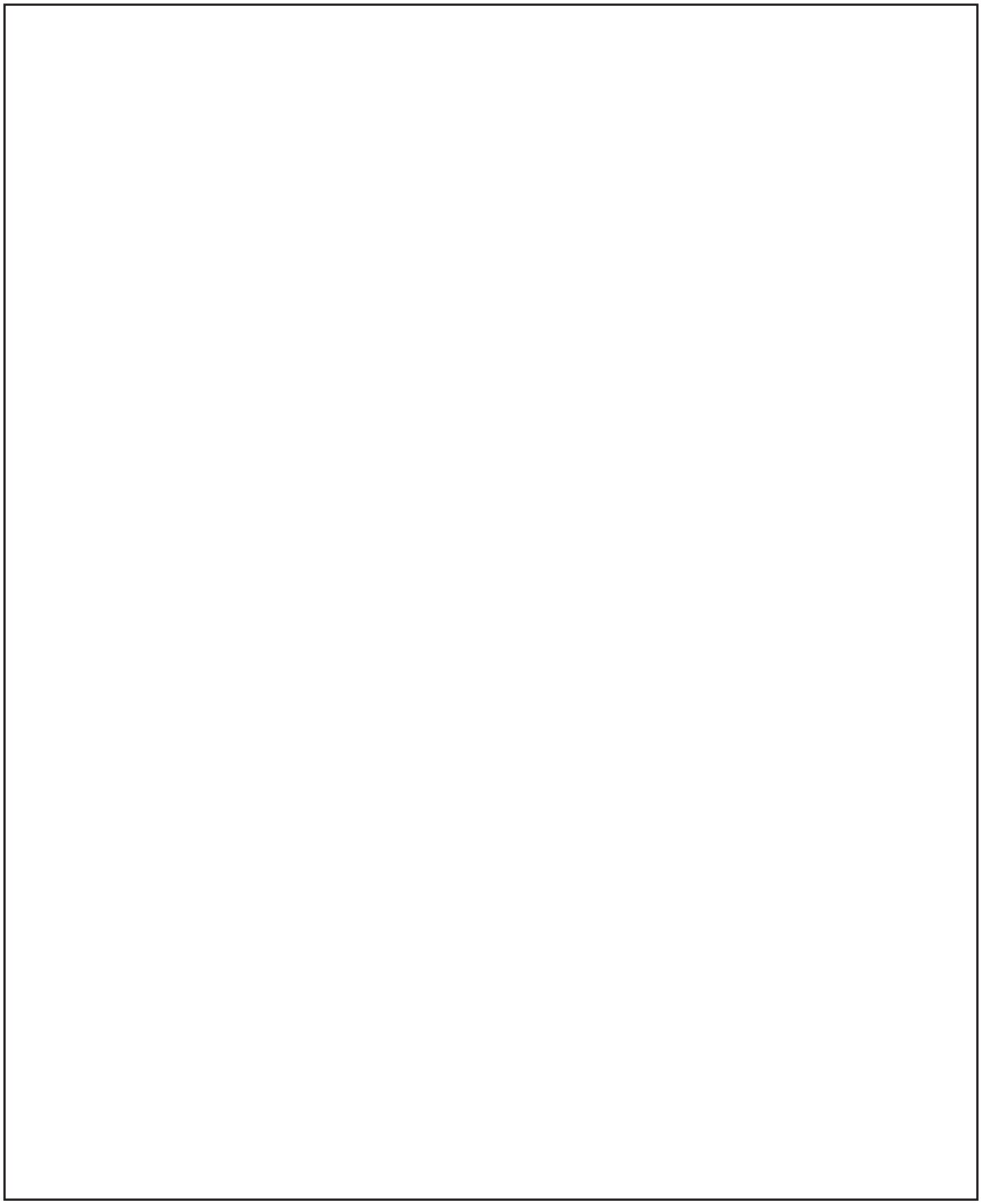

Figure 14. Bridge vibration characteristics and long period near-field motions. (a) Computed modeshapes (experimental values shown parenthetically); (b) Computed regional wave propagation at selected times; (c) Synthetic near-field ground motions.

Until very recently, the prevailing engineering wisdom has been that the lowest frequency, long wavelength modes of long-span bridges (e.g. the 9 second mode of the Bay Bridge) are generally not major contributors to the seismic response of the structure. Arguments offered in support of this view were based on the notion that the long period earthquake ground motions do not contain significant energy in the period range beyond 2 to 3 seconds, and that the time duration of a typical earthquake is too short to allow response build-up of these long period modes. However, the advent of broad-band digital strong motion instruments and the measurement of a number of near-field earthquake seismograms have challenged the traditional thinking. It is now clear that seismic wave radiation patterns and permanent co-seismic tectonic plate movements can result in large, long period ground displacement pulses and that these long period components can indeed excite the long wavelength modes of flexible bridge structures.

As an illustrative example of the potential effects of near field motions, the response of the Bay Bridge to eighty seconds of simulated ground motions has been computed. The simulated ground motions at the Bay Bridge site for a $M = 7$ Hayward Fault earthquake are shown in Figure (14) for selected support locations and the relative displacements across the bridge, as referenced to the Yerba Bucna Anchorage, are shown in Figure (15), (see Figure (1) for the Hayward fault proximity to the

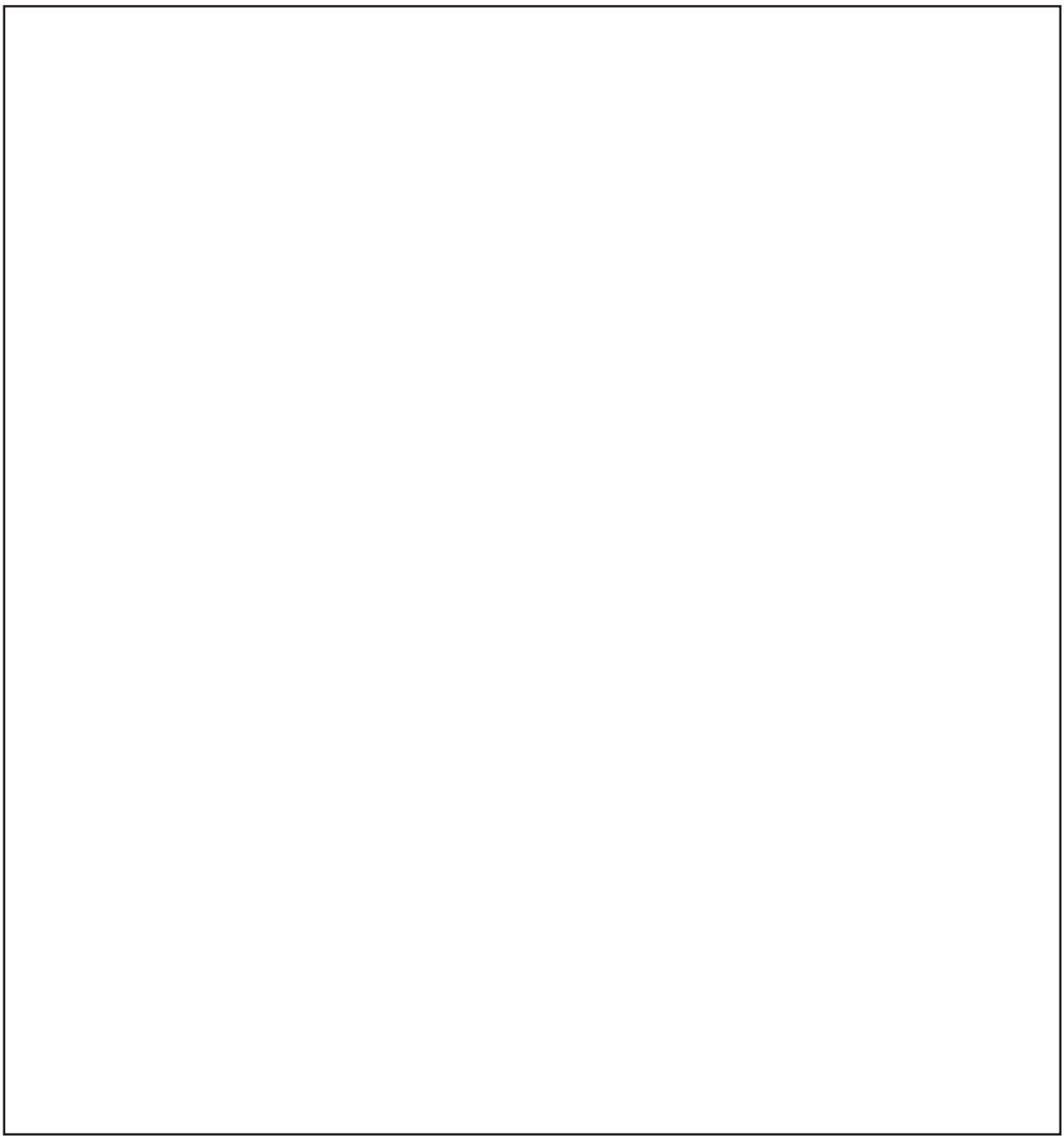

Figure 15. Near-field ground motions, (a) Comparison of Bay Bridge synthetic record with Chi-Chi earthquake measured record; (b) Relative motion across the bridge for the synthetic record.

bridge). These synthetic motions were computed with a massively parallel geophysics finite difference wave propagation model (Larsen and Schultz [27], Stidham et al [28]) and include long period displacement pulses and permanent ground displacements resulting from tectonic motions. The propagation of long period seismic waves across the region are also shown in Figure (14) at selected instants of time. For the particular bi-lateral rupture scenario considered, the ground motions exhibit a large displacement pulse transverse to the bridge structure with a permanent displacement offset resulting from tectonic motion. The relative displacements across the bridge exhibit a pulse with peak amplitude on the order of 75*cm* across the 3400*m* bridge. These synthetic ground motions were computed prior to the Chi-Chi earthquake in Taiwan and it is instructive to compare these records with some of the Chi-Chi measurements. Figure (15) shows an overlay of the synthetic Bay Bridge motion with a near-field Taiwan record and shows remarkably similar waveforms for the synthetic and real earthquakes.

The transient dynamic response of the bridge to this particular fault rupture scenario is shown in Figure (16). The exaggerated bridge displacements (displacement scale factor = 50) indicate that when the large displacement pulse occurs, the flexible deck cannot react as fast as the stiff towers and lags behind the tower motion, as the towers begin to return with the ground displacement in the opposite direction, the deck has finally begun to respond and essentially flings through the towers in the opposite direction. This type of motion imparts significant energy into the long wavelength modes right at the initiation of the earthquake motions, and is essential the same response phenomenon described for buildings subjected to long period motions by Hall et al [29, 30]. This rupture scenario, as well as a number of other fault rupture scenarios under study, indicate the important effect long period motions can play in the bridge response.

The global bridge model in Figure (16) contains 7600 degrees of freedom and time history compute times for 80 seconds of earthquake ground motion require approximately 7 hours for the full three dimensional simulations of the Bay Bridge system on a single processor Silicon Graphics Octane Workstation. This provides for over-night turnaround of relatively long time duration earthquake simulations for this large structure.

Figure 16. Response of the Bay Bridge system to the synthetic earthquake motions.

6. Conclusions

The special purpose of computational model which has been developed provides a powerful research tool for investigating the nonlinear dynamic response characteristics of suspension bridges. The specialized bridge elements allow practical exploitation of an explicit time integration solution of the equations of motion, which is a reliable and robust algorithm for highly nonlinear problems. The program can characterize a full bridge system with a modest number of global degrees of freedom and seismic simulation solution times on an desktop workstation are economical enough to allow efficient parametric studies. The explicit time integration provides a robust solution framework that will readily accommodate future implementation of complex nonlinear material behavior, such as laced member buckling and connection failures, and multiphysics capabilities such as direct coupling of fluid-structure interaction. Perhaps the most important aspect of the explicit integration framework is that it allows for easy migration of the *SUSPENDERS* program to the new generation of massively parallel computer. The fact that the explicit framework does not require a large matrix inversion, and essentially solves a set of "*n*" decoupled equations, makes parallel implementation straightforward. The next major planned development step for the *SUSPENDERS* program is a parallel implementation. It is projected that with new 1000+ processor class machines 80 second nonlinear earthquake simulations like those demonstrated here will be achievable on the order of 5-10 minutes of wall-clock time.

Acknowledgement

This work was funded by the University of California Directed Research and Development Fund. A portion of this work was performed at the Lawrence Livermore National Labortory under the auspices of the United States Department of Energy, contract no. W-7405-Eng-48.

REFERENCES

1. Abdel-Ghaffar, A.M. (1978). "Free Lateral Vibrations of Suspension Bridges", *Journal of the Structural Division, ASCE*, **104**(3), 503-525.

2. Abdel-Ghaffar, A.M. (1979). "Free Torsional Vibrations of Suspension Bridges", *Journal of the Structural Division, ASCE*, **105**(4), 767-788.

3. Abdel-Ghaffar, A.M. (1982). "Suspension Bridge Vibration: Continuum Formulation", *Journal of Engineering Mechanics, ASCE*, **108**(6), 1215-1231.

4. Dumanoglu, A.A., Brownjohn, J.M.W., and Severn, R.T. (1992). "Seismic Analysis of the Fatih Sultan Mehmet (Second Bosporus) Suspension Bridge", *Earthquake Engineering and Structural Dynamics*, **21**, 881-906.

5. Carder, D.S. (1937). "Observed Vibrations of Bridges", *Bulletin of the Seismological Society of America*, **29**(4), 267-303.

6. Abdel-Ghaffar, A.M. and Scanian, R.H. (1985). "Ambient Vibration Studies of Golden Gate Bridge: Suspended Structure' , *Journal of Engineering Mechanics, ASCE*, **111**(4), 463-482.

7. Abdel-Ghaffar, A.M. and Scanlan, R.H. (1985). "Ambient Vibration Studies of Golden Gate Bridge: Suspended Structure", *Journal of Engineering Mechanics, ASCE*, **111**(4), 483-499.

8. Brownjohn, J.M.W., Dumanoglu, A.A., and Severn, R.T. (1992). "Ambient Vibration Survey of the Fatih Sultan Mehmet (Second Bosporus) Suspension Bridge", *Earthquake Engineering and Structural Dynamics*, **21**, 907-924.

9. McLamore, V.R., Hart, G.C., and Stubbs, I.R. (1971). "Ambient Vibration of Two Suspension Bridges", *Journal of the Structural Division, ASCE*, **97**(10), 2567-2582.

10. Abdel-Ghaffar, A.M. and Rubin, L.I. (1983). "Nonlinear Free Vibrations of Suspension Bridges: Theory", *Journal of Engineering Mechanics, ASCE*, **109**(1), 313-329.

11. Abdel-Ghaffar, A.M. and Rubin, L.I. (1983). "Nonlinear Free Vibrations of Suspension Bridge: Application", *Journal of Engineering Mechanics, ASCE*, **109**(1), 330-345.

12. Nazmy, A.S. and Abdel-Ghaffar, A.M. (1990). "Non-Linear Earthquake Response of Long-Span Cable-Stayed Bridges: Theory", *Earthquake Engineering and Structural Dynamics*, **19**, 45-62.

13. Nazmy, A.S. and Abdel-Ghaffar, A.M. (1990). "Non-Linear Earthquake Response of Long-Span Cable-Stayed Bridges: Application", *Earthquake Engineering and Structural Dynamics*, **19**, 63-76.

14. Ingham, T.J., Rodriguez, S., and Nader, M. (1997). "Nonlinear Analysis of the Vincent Thomas Bridge for Seismic Retrofit", *Computers and Structures*, **64**(5/6), 1221-1238.

15. Wald, D.J. and Heaton, T.H. (1994). "Spatial and Temporal Distribution of Slip for the 1992 Landers-California, Earthquake", *Bulletin of the Seismological Society of America*, **84**(3), 668-691.

16. Loh, C.H., Lee, Z.K., Wu, T.C., and Peng, S.Y. (2000). "Ground Motion Characteristics of the Chi-Chi Earth-

quake of 21 September 1999", *Earthquake Engineering and Structural Dynamics*, **2000**(29), 867-897.

17. McCallen, D.B. and Astaneh-Asl, A. (1997). "*SUSPENDERS*: A Numerical Simulation Tool for the Nonlinear Transient Analysis of Cable Supported Bridge Structures Part I: Theoretical Development", *Lawrence Livermore National Laboratory Report UCRL-ID-127626*.

18. Cook, R.D., Malkus, D.S., and Plesha, M.E. (1989). "Concepts and Applications of Finite Elements", *John Wiley & Sons*.

19. Chopra, A.K. (1995). "Dynamics of Structures", Prentice-Hall.

20. Maker, B.N. (1995). "*NIKE3D*-A Nonlinear, Implicit Three-Dimensional Finite Element Code for Solid and Structural Mechanics", Lawrence Livermore National Laboratory Report UCRL-MA-105268 Rev. 1.

21. McCallen, D.B. and Romstad, K.M. (1990). "A Continuum Model for Lattice Structures with Geometric and Material Nonlinearities", *Computers and Structures*, **37**(5), 795-822.

22. Avent, R.R. and Issa, R.R. (1982). "Beam Element Stiffness Matrix for X-Braced Truss", *ASCE Journal of Structural Division*, **108**(10), 2192-2210.

23. Astaneh-Asl, A., Cho, S.W., Bowen, C.M., and Blondet, M. (1993). "Post-Buckling Ductility of Critical Members of the Golden Gate Bridge", University of California at Berkeley Report UCB/CE-Stell-93/01.

24. Irvine, H.M. and Sinclair, G.B. (1976). "The Suspended Elastic Cable under the Action Concentrated Vertical Loads", *International Journal of Solids and Structures*, **12**, 309-317.

25. Malhotra, P.K., Huang, M.J., and Shakal, A.F. (1995). "Seismic Interaction at Separation Joints of an Instrumented Concrete Bridge", *Earthquake Engineering and Structural Dynamics*, **24**, 1055-1067.

26. McCallen, D.B. and Romstad, K.M. (1994). "Nonlinear Model for Building-Soil Systems", *Journal of Engineering Mechanics, ASCE*, **120**(5), 1129-1152.

27. Larsen, S.C. and Schultz, C.A. (1995). "ELAS3D:2D/3D Elastic Finite Difference Wave Propagation Code", *Lawrence Livermore National Laboratory Report UCRL-MA-121729.*

28. Stidham, C., Antolik, M., Dreger, D., Larsen, S., and Romanowicz, B. (1999). "Three Dimensional Structure Influences on the Strong-Motion Wavefield of the 1989 Loma Prieta Earthquake", *Bulletin of the Seismological Society of America*, **89**(5), 1184-1202.

29. Hall, J.F., Heaton, T.H., Halling, M.W., and Wald, D.J. (1995). "Near-Source Ground Motion and its Effects on Flexible Buildings", EERI Earthquake Specra, **11**.

30. Heaton, T.H., Hall, J.F., Wald, D.J., and Halling, M.W. (1995). "Response of High-Rise and Base-Isolated Buildings to a Hypothetical Mw 7.0 Blind Thrust Earthquake", *Science*, **267**.